Vol. 48, No. 3 (2026) 595-614, DOI: 10.24874/ti.2205.05.26.07

Tribology in Industry

www.tribology.rs

RESEARCH

Comparative Optical Roughness Measurement of Mild Steel Ship Plates Using a Microscope and DSLR Imaging

Eko Sasmito Hadi[a,*], Muhammad Raaflie Caesar Putra Hadi[a], Muhammad Luqman Hakim[a], M. Dafa Maziya[a], J. Jamari[b]

[a]*Department of Naval Architecture, Faculty of Engineering, Diponegoro University, Jl. Prof Sudharto, Tembalang, Semarang, Central Java 50275, Indonesia,*
[b]*Laboratory for Engineering Design and Tribology, Faculty of Engineering, Department of Mechanical Engineering, Diponegoro University, Indonesia.*

Keywords:

Surface roughness
Optical roughness measurement
Non-contact metrology
Surface characterization
Mild steel ship plates

* Corresponding author:

Eko Sasmito Hadi
E-mail: ekosasmito@ft.undip.ac.id

Received: 4 May 2026
Revised: 1 June 2026
Accepted: 6 July 2026

A B S T R A C T

Surface roughness of ship plates is an important surface parameter because it influences coating condition, fouling development, hydrodynamic resistance, and maintenance decisions. However, this study does not directly measure friction, wear, lubrication, or tribological performance. Instead, it evaluates optical roughness measurement as a supporting method for roughness-based surface inspection of marine steel surfaces. This study compares two non-contact optical imaging systems, a metallurgical microscope and a DSLR camera, for estimating the roughness parameters Ra and Rz of mild steel ship plates. Validation was performed using eight ISO 2632 reference surfaces with certified Ra values ranging from 0.05 to 0.40 µm. Roughness values were processed using Gwyddion and ImageJ, and the DSLR system was evaluated at five camera–surface distances of 1, 2, 3, 4, and 5 cm. All tested configurations achieved validation accuracy above 91% for both Ra and Rz. The microscope showed the highest overall agreement with the certified reference values, while Gwyddion yielded results closer to the certified reference values than ImageJ. In the DSLR workflow, measurement accuracy decreased with increasing camera–surface distance, underscoring the importance of controlled imaging geometry. An application to a mild steel plate showed that both systems could detect small differences in roughness, although the microscope resolved local surface features more clearly. These results indicate that calibrated optical imaging can support the assessment of roughness on fine mild steel surfaces under controlled conditions. However, because the validation range was limited to fine reference surfaces, further validation is required before applying the workflow to blasted, corroded, coated, or fouled ship surfaces. DSLR imaging may be useful as a screening-level approach, but its reliability depends on controlled distance, illumination, focus, exposure, and calibration.

1. INTRODUCTION

Surface roughness is an important surface parameter for ship hull plates because it is related to hydrodynamic resistance, coating condition, fouling development, and maintenance planning. Changes in surface topography can alter near-wall flow behavior, increase frictional resistance, and reduce vessel efficiency over time. In marine service, roughness also interacts with coating degradation and biofouling, which can further affect drag, fuel consumption, and emissions [1–6]. Recent studies have further shown that hull roughness caused by corrosion, coating degradation, and biofouling can increase ship resistance, reduce speed performance, and increase energy demand [7,8]. Local or non-uniform hull roughness may also affect resistance and fuel consumption differently depending on its position on the wetted surface [9]. Therefore, roughness measurement is useful for marine surface inspection and maintenance decision-making.

However, this study does not directly measure friction, wear, lubrication, or tribological performance. Instead, it focuses on optical roughness measurement and surface characterization as supporting tools for tribology-relevant inspection of marine steel surfaces. In this context, roughness is treated as a measurable surface descriptor that can help evaluate surface condition, coating readiness, and maintenance needs, rather than as a direct indicator of tribological performance.

In practice, surface roughness in shipyard and maintenance environments is still commonly assessed using stylus profilometers. Although this technique is well established, it has several limitations for marine applications. Contact measurements may damage soft coatings or sensitive surface layers, sampling is local rather than area-based, and measurements over large or geometrically complex hull surfaces can be difficult to perform efficiently. Probe wear, positioning errors, and thermal drift may also reduce measurement reliability under less controlled conditions [10–12]. These limitations encourage the development of non-contact approaches to support faster, less invasive surface assessment [13].

Optical non-contact methods have therefore gained attention for the characterization of metallic surfaces. Confocal microscopy has shown good agreement with contact-based methods while offering sensitivity to fine topographical features on reflective surfaces [14,15]. Fringe projection profilometry and laser-based optical methods have also shown potential for quantitative roughness assessment when calibration and acquisition conditions are carefully controlled [16–18]. In addition, image-based and camera-assisted approaches offer practical advantages because they are lower-cost, more portable, and easier to deploy than laboratory profilometry systems. Recent image-processing-based roughness evaluation has shown that surface images can be used to estimate roughness when image features are calibrated against reference measurements. However, such approaches remain sensitive to image acquisition, feature extraction, and model calibration [19].

Despite these developments, several gaps remain for marine steel inspection. Many previous studies have focused on polished, machined, or non-marine specimens, while validation on mild steel surfaces relevant to ship plates remains limited. The performance of low-cost DSLR-based imaging for roughness estimation remains underreported, especially when compared directly with microscope-based imaging within the same reference validation framework. In addition, the effects of camera–surface distance and image-processing workflow on roughness estimation remain insufficiently clarified for marine engineering applications [15,16,20].

The novelty of this study lies in the direct comparison of microscope- and DSLR-based optical imaging for estimating Ra and Rz on shipbuilding-relevant mild steel, using a unified ISO 2632 reference validation framework, distance-dependent DSLR assessment, and parallel evaluation of Gwyddion and ImageJ processing workflows. This combination provides a practical basis for evaluating whether accessible optical imaging systems can support roughness-based inspection of mild steel surfaces under controlled conditions.

Accordingly, this study investigates the feasibility of non-contact optical measurement of the roughness of mild steel ship plates using two imaging configurations: a metallurgical microscope and a DSLR camera. The study is guided by the hypothesis that calibrated optical imaging can reproduce standard roughness parameters with high agreement. At the same time, the microscope is expected to outperform the DSLR due to its higher optical resolution and more stable imaging configuration. The main objective is to compare the accuracy of microscope- and DSLR-based roughness estimation for Ra and Rz and to evaluate the effects of camera–surface distance and image-processing workflow.

The validation range of this study is limited to fine reference surfaces with Ra values from 0.05 to 0.40 μm. Therefore, the present findings should not be directly generalized to blasted, corroded, coated, or fouled ship plates without additional validation. By recognizing this limitation, the study positions the proposed optical workflow as a controlled-condition method for roughness-based surface characterization of fine or finished mild steel surfaces, rather than as a direct replacement for standard industrial profilometry.

2. METHODOLOGY

2.1 Research design and experimental framework

This study used a controlled laboratory experiment to evaluate the feasibility and accuracy of non-contact optical roughness measurement on mild steel ship plates. The experimental design was structured to assess three main factors: imaging device, camera–surface distance, and image-processing software. The imaging device comparison was performed between a metallurgical microscope and a Nikon D3300 DSLR camera. The effect of camera–surface distance was evaluated for the DSLR system at distances of 1, 2, 3, 4, and 5 cm. The software comparison was performed between Gwyddion and ImageJ.

Validation was conducted using an ISO 2632 roughness comparison plate as the reference artifact. The certified Ra and Rz values of the reference plate were used to assess the agreement between the optical measurements and the standard values. Therefore, the validation in this study establishes the performance of the optical workflow against a certified reference plate. However, no direct stylus profilometer measurement was performed on the same mild steel specimen. This limitation means that the present study does not yet demonstrate full equivalence between the optical workflow and standard industrial roughness measurement on the actual shipbuilding steel substrate.

The validation in this study should be interpreted as agreement with the certified ISO 2632 roughness comparison plate. It does not establish full equivalence with stylus profilometry or industrial optical profilometry on the same mild steel specimen. Therefore, the proposed workflow is evaluated as a controlled-condition approach for optical roughness measurement.

For the DSLR validation workflow, five replicate images were acquired for each reference surface at each camera–surface distance. For the mild steel case study, ten images were acquired for each specimen condition, and roughness was evaluated along five independent measurement lines. Microscope-based measurements were obtained from the same certified reference surfaces under fixed imaging conditions to ensure consistency with the DSLR validation framework. All repeated measurements were summarized as mean ± standard deviation to describe both the central tendency and variability of the optical roughness estimates.

The overall workflow consisted of five stages: reference surface preparation, optical image acquisition, image calibration and processing, roughness parameter extraction, and validation against the certified ISO 2632 values. The same validation framework was applied to both Ra and Rz. After validation using the reference plate, the optical workflow was applied to the mild steel plate to evaluate whether both imaging systems could detect local roughness differences on a shipbuilding-relevant steel surface.

2.2 Materials, reference standards, and optical instruments

The test material was a mild steel plate representative of low-carbon shipbuilding steel (C < 0.3%), obtained from the Naval

Architecture Engineering Welding Laboratory. Validation was performed using an ISO 2632 roughness comparison plate In size 18071116 containing eight certified surface conditions: Flat Lapping 3 Ra 0.05 µm; Rz 0.55 µm, Flat Lapping 2 Ra 0.10 µm; Rz 1.00 µm, Flat Lapping 1 Ra 0.20 µm; Rz 1.60 µm, Grinding 6 Ra 0.40 µm; Rz 3.00 µm, Grinding 5 Ra 0.05 µm; Rz 0.55 µm, Reaming 3 Ra 0.10 µm; Rz 1.00 µm, Turning 6 Ra 0.40 µm; Rz 2.50 µm, and Horizontal Milling 6 Ra 0.40 µm; Rz 2.50 µm. These surfaces cover a certified range of Ra = 0.05–0.40 µm and Rz = 0.55–3.00 µm.

The ISO 2632 roughness comparison plate (Insize 18071116), shown in Figure 1, was used as the primary validation artifact in this study. It consists of eight machined reference surfaces representing flat lapping, grinding, reaming, turning, and horizontal milling conditions. The certified Ra and Rz values of these surfaces, listed in Table 1, were used as reference values for the accuracy assessment.

Two optical systems were used. The first was a metallurgical trinocular microscope equipped with a 10× eyepiece and plan-achromatic long-working-distance objectives of 5×/0.12, 10×/0.25, 40×/0.60, 60×/0.75, and 100×/0.85. The second was a Nikon D3300 DSLR camera with a 24.2 MP CMOS sensor (23.2 × 15.4 mm, 6000 × 4000 pixels), operated in macro mode. Roughness extraction and data processing were performed using Gwyddion and ImageJ. Gwyddion was used for calibration, leveling, filtering, and ISO-style profile parameter extraction, whereas ImageJ was used as an intensity-based alternative workflow for camera image analysis [21,22].

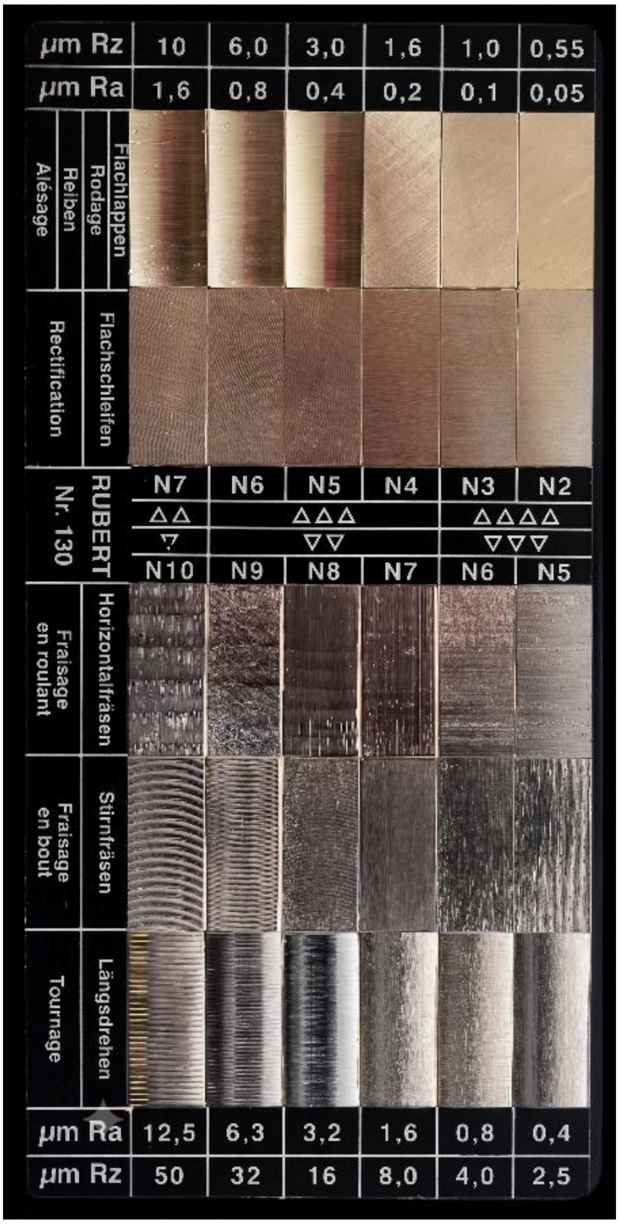

Fig. 1. ISO 2632 roughness comparison plate (Insize 18071116) used as the validation artifact, containing eight certified reference surfaces with Ra and Rz values used for accuracy assessment.

Table 1. Standard roughness parameters Ra and Rz in µm of the ISO 2632 validation plate surfaces, including manufacturing process, ISO roughness grade, and technical surface quality code.

No.	Manufacturing Process	ISO Roughness Grade	Ra [µm]	Rz [µm]	Technical Surface Quality Code
1	Flat Lapping / Reaming	N2	0.05	0.55	∇∇∇∇
2	Flat Lapping / Reaming	N3	0.10	1.00	∇∇∇
3	Flat Lapping / Reaming	N4	0.20	1.60	∇∇∇
4	Grinding	N5	0.40	3.00	∇∇∇
5	Grinding	N2	0.05	0.55	∇∇∇∇
6	Flat Lapping / Reaming	N3	0.10	1.00	∇∇∇
7	Turning	N5	0.40	2.50	∇∇∇
8	Horizontal Milling	N5	0.40	2.50	∇∇∇

The Grinding N2 surface has the same certified Ra and Rz values as the Flat Lapping / Reaming N2 surface. This value was retained because it corresponds to a separate reference track on the ISO 2632 comparison plate and was verified from the reference plate information.

2.3 Experimental conditions and image acquisition

Two optical imaging systems were used in this study: a metallurgical trinocular microscope and a Nikon D3300 DSLR camera. The microscope was used as the higher-resolution laboratory imaging system, whereas the DSLR camera was evaluated as a lower-cost and more portable imaging alternative. Both systems were used to acquire images of the ISO 2632 roughness comparison plate and the mild steel specimen under controlled laboratory conditions.

For microscope imaging, a 40× plan-achromatic long-working-distance objective with a numerical aperture of 0.60 was used. The observation angle was maintained at approximately 30° relative to the optical axis. This configuration was selected to maintain stable focus and sufficient contrast while preserving a realistic inspection geometry. The light intensity at the specimen plane ranged from 262 to 286 lux, depending on the reference surface. The microscope imaging settings are summarized in Table 2.

For DSLR imaging, the Nikon D3300 was set to macro mode. Images were acquired at five camera–surface distances, namely 1, 2, 3, 4, and 5 cm. The aperture and shutter speed were kept constant at f/8 and 1/100 s, respectively. ISO sensitivity was adjusted to compensate for distance-related exposure changes: ISO 400 at 1–2 cm, ISO 600 at 3 cm, and ISO 800 at 4–5 cm. For the DSLR validation workflow, five replicate images were acquired for each certified reference surface at each camera–surface distance. For the mild steel case study, ten images were acquired for each specimen condition [23-25]. The DSLR imaging settings are summarized in Table 3.

Table 2. Microscope imaging settings for each validation surface, including objective magnification, numerical aperture, tilt angle, and light intensity at the specimen plane.

Specimen	Magnification	Objective	Tilt Angle [°]	Light Intensity [lux]
Flat Lapping 3	Plan Achromatic 40×	NA 0.60 LWD*	30	286
Flat Lapping 2	Plan Achromatic 40×	NA 0.60 LWD	30	262
Flat Lapping 1	Plan Achromatic 40×	NA 0.60 LWD	30	273
Grinding 6	Plan Achromatic 40×	NA 0.60 LWD	30	268
Grinding 5	Plan Achromatic 40×	NA 0.60 LWD	30	263
Reaming 3	Plan Achromatic 40×	NA 0.60 LWD	30	279
Turning 6	Plan Achromatic 40×	NA 0.60 LWD	30	264
Horizontal Milling 6	Plan Achromatic 40×	NA 0.60 LWD	30	274

Table 3. DSLR camera settings for image acquisition at different camera–surface distances, including ISO, aperture, shutter speed, and light intensity.

Distance [cm]	ISO	Aperture f/stop	Shutter Speed [s]	Light Intensity [lux]
1	400	f/8	1/100	68
2	400	f/8	1/100	66
3	600	f/8	1/100	65
4	800	f/8	1/100	63
5	800	f/8	1/100	61

The effective spatial resolution of the DSLR images was determined from the calibrated field of view at each camera–surface distance. The field of view was obtained from the spatial calibration of each image using the reference plate geometry. The effective spatial resolution was calculated by dividing the calibrated field of view by the image size in pixels. The horizontal and vertical spatial resolutions were calculated as follows:

$$\textbf{Effective spatial resolution x} = \frac{FOV_x}{N_x} \quad (1)$$

$$\textbf{Effective spatial resolution y} = \frac{FOV_y}{N_y} \quad (2)$$

where FOVx and FOVy are the calibrated horizontal and vertical field of view values in µm, and Nx and Ny are the horizontal and vertical pixel numbers of the image, respectively. For the Nikon D3300 images used in this study, the image size was 6000 × 4000 pixels.

The DSLR workflow is sensitive to imaging conditions. Increasing the camera-surface distance reduces the effective spatial sampling of fine surface features, thereby smoothing local asperities and reducing the accuracy of roughness estimation. In addition, focus stability, illumination uniformity, exposure setting, surface reflectivity, and glare may influence the contrast and texture information extracted from metallic surfaces. These factors are particularly important for reflective steel surfaces and for possible field use, where lighting, distance, camera angle, and surface cleanliness are more difficult to control than in laboratory conditions. Therefore, the DSLR system should be interpreted as a screening-level imaging approach under controlled acquisition conditions.

The effective spatial resolution of the DSLR images was calculated from the calibrated region of interest used for roughness analysis. In this study, the same calibrated field of view (region of interest) of 10 mm × 10 mm was used for all DSLR camera–surface distances. With an image size of 6000 × 4000 pixels, the effective spatial resolution was 1.67 µm/pixel horizontally and 2.50 µm/pixel vertically. The mean effective spatial resolution was therefore 2.08 µm/pixel.

Table 4. DSLR field of view and effective spatial resolution at different camera–surface distances, calculated using the same calibrated ROI of 10 mm × 10 mm.

Distance [cm]	Image Size [pixels]	Field of View [mm × mm]	Effective Spatial Resolution [µm/pixel]	Mean Effective Spatial Resolution [µm/pixel]
1	6000 × 4000	10 × 10	1.67 × 2.50	2.08
2	6000 × 4000	10 × 10	1.67 × 2.50	2.08
3	6000 × 4000	10 × 10	1.67 × 2.50	2.08
4	6000 × 4000	10 × 10	1.67 × 2.50	2.08
5	6000 × 4000	10 × 10	1.67 × 2.50	2.08

As shown in Table 4, the same calibrated region of interest was used for all DSLR distances; therefore, the calculated effective spatial resolution remained constant across the five tested camera–surface distances. The effective spatial resolution was 1.67 µm/pixel horizontally and 2.50 µm/pixel vertically, with a mean of 2.08 µm/pixel.

Because the calculated effective spatial resolution remained constant, the decrease in DSLR measurement accuracy with increasing distance should be interpreted cautiously. In this study, the decrease was primarily attributable to distance-dependent optical effects, including focus stability, image sharpness, illumination uniformity, surface contrast, and exposure variation, rather than to changes in the calculated spatial resolution. These factors may affect image-based roughness estimation on reflective metallic surfaces by reducing the visibility of fine asperities and valleys and producing smoother reconstructed roughness profiles [26-28].

Therefore, the DSLR-based workflow should be considered a controlled-condition and screening-level approach. Although the calibrated spatial resolution was constant within the selected region of interest, reliable roughness estimation still requires consistent focus, illumination, exposure, and surface contrast during image acquisition [26–28].

2.4 Image processing and roughness parameter extraction

Image processing was performed using two workflows: Gwyddion and ImageJ. Gwyddion was used as the primary workflow because it supports spatial calibration, leveling, filtering, profile extraction, and roughness parameter calculation. ImageJ was used as an alternative intensity-based workflow, leveraging grayscale and texture information. Therefore, ImageJ-derived roughness values were interpreted as indirect optical estimates rather than direct topographical measurements [15,17,21,22].

The optical images were spatially calibrated before roughness extraction. Microscope images were calibrated based on optical magnification and image resolution, while DSLR images were calibrated using the known field of view and image size. For the DSLR workflow, the calibrated field of view was 10 mm × 10 mm, and the image size was 6000 × 4000 pixels. This resulted in an effective spatial resolution of 1.67 µm/pixel horizontally and 2.50 µm/pixel vertically, with a mean value of 2.08 µm/pixel.

The DSLR images were treated as reference-calibrated optical texture maps, not as direct three-dimensional topography maps. The extracted intensity and texture information were calibrated against the certified Ra and Rz values of the ISO 2632 roughness comparison plate. Therefore, DSLR-derived roughness values were interpreted as calibrated optical roughness estimates that depend on imaging distance, focus, illumination, surface reflectivity, and calibration quality [15,1,26,27].

The DSLR and ImageJ workflows were interpreted as reference-calibrated estimates of optical roughness rather than as direct three-dimensional topographical measurements. Their reliability depends on image quality, spatial calibration, focus stability, illumination uniformity, exposure setting, threshold selection, and surface reflectivity. Therefore, these workflows should be used within the validated reference range and under controlled acquisition conditions.

The conversion process followed a reference-based calibration approach. Images of the ISO 2632 reference surfaces were acquired under controlled conditions, spatially calibrated, processed to extract optical texture and profile-like intensity variations, and then compared with the certified Ra and Rz values. The calibrated workflow was subsequently applied to the mild steel specimen within the validated reference range [17,21,29].

This approach does not mean that a conventional DSLR image directly contains complete height information. Instead, roughness was estimated from a calibrated relationship between optical image features and certified reference roughness values. Similar image-processing-based methods for roughness estimation have been reported previously [19]. Therefore, the DSLR and ImageJ results were interpreted as reference-calibrated estimates rather than direct replacements for stylus or industrial optical profilometry [15,30].

In Gwyddion, each calibrated image underwent spatial calibration, leveling, Gaussian filtering, profile extraction, and roughness parameter calculation. Leveling and field correction were used to reduce tilt and background effects, while Gaussian filtering with a cut-off wavelength of λc = 0.8 mm was applied to separate roughness from longer-wavelength surface variation. Ra and Rz were then calculated from the filtered profiles in accordance with ISO 4287 and ISO 4288 [17,21,29].

Gwyddion was considered the primary processing workflow because it offers a more structured, profile-based approach to roughness analysis. Its ability to apply calibration, leveling, filtering, and profile extraction makes it more suitable for quantitative roughness estimation than a purely intensity-based workflow [17,21].

In the ImageJ workflow, the images were processed as indirect intensity-based roughness estimates rather than direct topographical measurements. Each image was imported, converted to 8-bit grayscale, and cropped to a consistent region of interest. Contrast adjustment and threshold-based segmentation were then applied to isolate surface texture features. Grayscale and texture-related descriptors were extracted from each ROI and calibrated against the certified Ra and Rz values of the ISO 2632 reference surfaces. A separate linear calibration model was used for Ra and Rz, expressed as $Ra = a_1D + b_1$ and $Rz = a_2D + b_2$, where D is the selected ImageJ descriptor and a and b are calibration coefficients obtained from the reference plate. Because ImageJ does not reconstruct a calibrated height map, the resulting values were interpreted as indirect intensity-based roughness estimates. This workflow is sensitive to illumination, threshold selection, image contrast, focus, camera–surface distance, and surface reflectivity.

Therefore, ImageJ was used as a low-cost screening workflow, while Gwyddion was used as the primary workflow for extracting profile-based roughness parameters [19].

For the mild steel plate, roughness was sampled along five independent measurement lines for each imaging system. The same calibration and processing sequence was applied to compare microscope- and DSLR-derived results. However, because the DSLR and ImageJ workflows rely on optical image features, their results should be interpreted within the validated reference range and under controlled imaging conditions.

2.5 Validation and accuracy assessment

Validation was performed by comparing the measured Ra and Rz values with the certified values of the ISO 2632 roughness comparison plate shown in Figure 1 and Table 1. The validation included eight certified reference surfaces. For each surface, roughness values were obtained from microscope- and DSLR-based images after image processing. In the DSLR workflow, five replicate images were acquired at each camera–surface distance for each certified surface. For the mild steel case study, ten images were acquired for each specimen condition, and roughness was evaluated along five independent measurement lines.

All replicate measurements were reported as mean ± standard deviation. The mean value represented the measured roughness under each condition, while the standard deviation described measurement variability and was used for error-bar presentation.

Measurement accuracy was calculated as follows:

$$\text{Accuracy}(\%) = \left[1 - \frac{|R_{\text{meas}} - R_{\text{std}}|}{R_{\text{std}}}\right] \times 100 \qquad (3)$$

where R_{meas} is the measured roughness value and R_{std} is the certified reference value. This equation was applied separately to Ra and Rz.

To strengthen the validation, additional performance metrics were calculated, including mean absolute error (MAE), root mean square error (RMSE), bias, mean absolute percentage error (MAPE), and the coefficient of determination (R^2). These metrics were used to evaluate the magnitude of errors, error direction, relative deviation, and agreement between measured and certified values across the eight ISO 2632 reference surfaces.

$$\text{MAE} = \frac{1}{n}\sum |\, R_{\text{meas},i} - R_{\text{std},i} \,| \qquad (4)$$

$$\text{RMSE} = \sqrt{\frac{1}{n}\sum (R_{\text{meas},i} - R_{\text{std},i})^2} \qquad (5)$$

$$\text{Bias} = \frac{1}{n}\sum (R_{\text{meas},i} - R_{\text{std},i}) \qquad (6)$$

$$\text{MAPE}(\%) = \frac{1}{n}\sum \left| \frac{R_{\text{meas},i} - R_{\text{std},i}}{R_{\text{std},i}} \right| \times 100 \qquad (7)$$

$$R^2 = 1 - \frac{\sum (R_{\text{meas},i} - R_{\text{std},i})^2}{\sum (R_{\text{std},i} - \bar{R}_{\text{std}})^2} \qquad (8)$$

where $R_{\text{meas},i}$ is the measured roughness value for the i-th reference surface, $R_{\text{std},i}$ is the corresponding certified value, $\bar{R}_{\text{std}}$ is the mean certified value, and n is the number of reference surfaces. In this study, $n = 8$.

Statistical analysis was performed to assess differences among imaging devices, camera-surface distances, and image-processing workflows. Microscope versus DSLR measurements and Gwyddion versus ImageJ measurements were treated as paired comparisons because the same certified reference surfaces were used. The effect of DSLR camera-surface distance was evaluated at distances of 1, 2, 3, 4, and 5 cm.

Data normality was assessed before statistical testing. For normally distributed data, paired t-tests were used for two-group comparisons, while one-way ANOVA or repeated-measures ANOVA was used to evaluate distance effects. If normality was not satisfied, the Wilcoxon signed-rank test and the Friedman test were used as nonparametric alternatives. Statistical significance was set at $p < 0.05$.

The use of a certified roughness artifact aligns with the principle of performance assessment through calibrated material measures and reference standards. In surface texture metrology, material measures are commonly used for instrument calibration and performance verification. Therefore, in this study, the ISO 2632 roughness comparison plate was used as a certified reference artifact to evaluate the agreement between the optical measurements and the certified Ra and Rz values, rather than to establish a complete uncertainty budget [30,31].

After reference-based validation, the same processing and evaluation workflow was applied to the mild steel plate to assess the optical systems' sensitivity to local variations in roughness. However, because no direct stylus profilometer measurement was performed on the same mild steel specimen, the validation should be interpreted as agreement with the ISO 2632 reference plate rather than full equivalence with standard industrial roughness instruments.

3. RESULTS

3.1 Effect of image capture device on roughness measurement

All figures and tables in this section are cited and interpreted in the main text. Figures are used to visualize measurement trends, accuracy comparisons, roughness maps, profile differences, and the conceptual workflow, while tables summarize reference values, acquisition settings, validation metrics, and comparative performance. Where repeated measurements were performed, values are reported as mean ± standard deviation, and error bars represent measurement variability.

The roughness values obtained from the metallurgical microscope and Nikon D3300 DSLR were validated against eight ISO 2632 reference surfaces and reported as mean ± standard deviation. The error bars in Figures 2 and 3 represent measurement variability under each imaging condition.

Both systems showed good agreement with the certified Ra and Rz values. For the Flat Lapping 3 surface, the certified values were Ra = 0.05 μm and Rz = 0.55 μm. The microscope measured Ra = 0.0477 μm and Rz = 0.5144 μm, while the DSLR measured Ra = 0.0473 μm and Rz = 0.5139 μm. These results indicate slight underestimation by both systems, with the microscope showing closer agreement with the reference values.

The microscope's higher accuracy is attributed to its more stable optical configuration and greater ability to resolve fine peak-and-valley features. The 40× objective with an NA of 0.60 improved detection of surface detail, whereas the DSLR workflow was more sensitive to focus stability, illumination uniformity, surface reflectivity, and image sharpness. These factors can reduce the visibility of fine asperities and produce smoother reconstructed profiles, particularly for sub-micrometer roughness on reflective metallic surfaces [22–24].

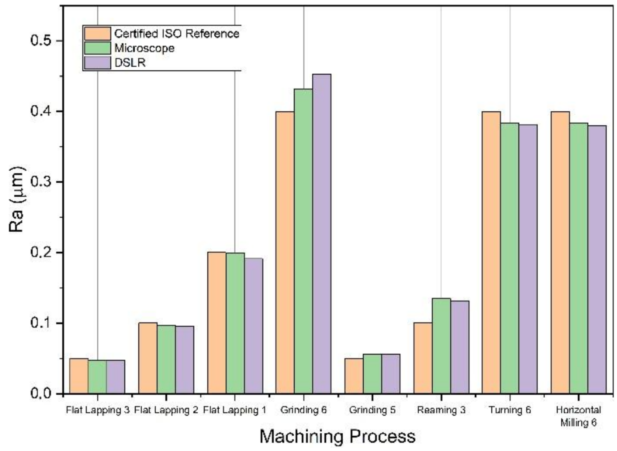

(a)

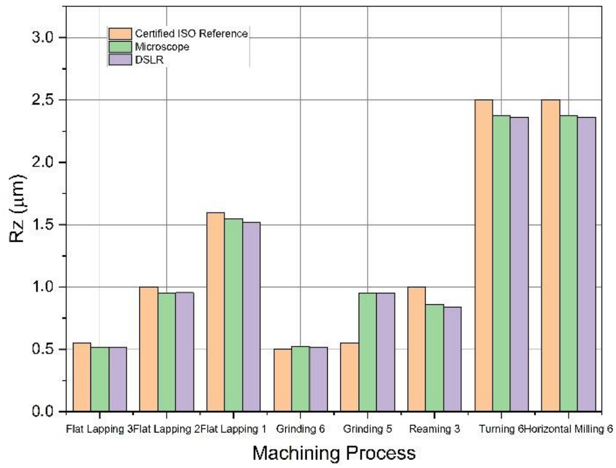

(b)

Fig. 2. Comparison of certified and measured roughness values obtained using microscope and DSLR imaging across eight ISO 2632 reference surfaces: (a) Ra and (b) Rz. Values are reported as mean ± standard deviation, where replicate measurements were available.

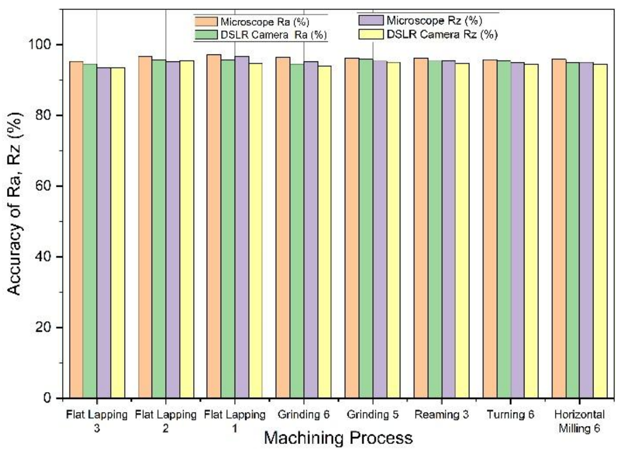

Fig. 3. Percentage accuracy of Ra and Rz measurements obtained using microscope and DSLR imaging relative to the ISO 2632 certified reference values. Error bars represent the standard deviation from repeated measurements.

To summarize the device-based comparison, Table 5 presents the certified roughness range, representative measured values, accuracy ranges, and main interpretation for the microscope and DSLR workflows. The summary shows that both systems reproduced the ISO 2632 reference values with good agreement, but the microscope produced slightly closer agreement with the certified Ra and Rz values.

As shown in Table 5, the microscope provided slightly higher accuracy than the DSLR for both Ra and Rz. This difference is attributed to the microscope's higher optical resolution and more stable imaging configuration, which allows finer peak-and-valley features to be captured more clearly. In contrast, DSLR measurements remained reliable but were more sensitive to focus, illumination, surface reflectivity, and image sharpness. Therefore, the microscope is better suited to detailed quantitative roughness assessment, whereas the DSLR is better suited to controlled screening-level evaluation.

Table 5. Summary of device-based roughness measurement performance, showing certified range, representative measured value, accuracy range, and main interpretation for microscope and DSLR workflows.

Device	Param.	Cert. Range [μm]	Rep. Value [μm]	Acc. Range [%]	Main Note
Microscope	Ra	0.05–0.40	0.0477	95.31–97.20	Highest agreement
Microscope	Rz	0.55–3.00	0.5144	93.53–96.72	Better peak–valley resolution
DSLR	Ra	0.05–0.40	0.0473	94.58–95.86	Good screening accuracy
DSLR	Rz	0.55–3.00	0.5139	93.44–95.45	Slightly smoother reconstruction

Overall, microscope-based measurements achieved Ra accuracies of 95.31–97.20% and Rz accuracies of 93.53–96.72%, while DSLR-based measurements achieved Ra accuracies of 94.58–95.86% and Rz accuracies of 93.44–95.45%. Thus, the microscope is more suitable for detailed quantitative assessment of roughness, whereas the DSLR remains useful for controlled screening-level evaluation.

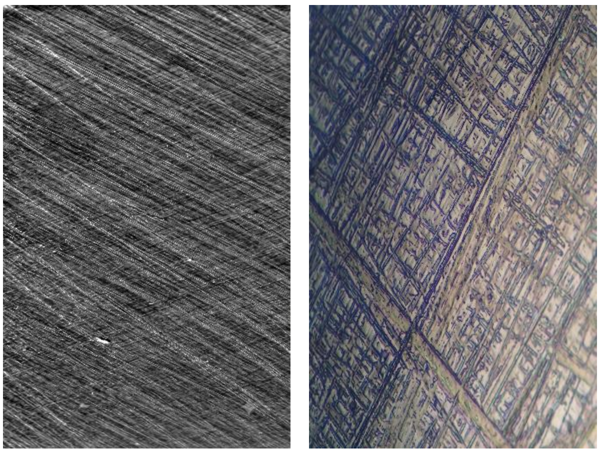

(a) (b)

Fig. 4. Representative roughness maps reconstructed from (a) DSLR and (b) microscope images, showing smoother DSLR reconstruction and sharper peak-and-valley features in the microscope-based map.

Figure 4 supports this interpretation, showing sharper peak-and-valley features in the microscope-based map and a smoother texture representation in the DSLR-based map.

3.2 Effect of image capture distance on roughness accuracy

The effect of camera–surface distance on DSLR-based roughness estimation was evaluated at distances of 1, 2, 3, 4, and 5 cm. Figure 5 presents the Ra values obtained at each distance for the eight ISO 2632 reference surfaces, while Figure 6 shows the corresponding accuracy values. The results indicate a gradual decrease in DSLR accuracy as the camera–surface distance increased.

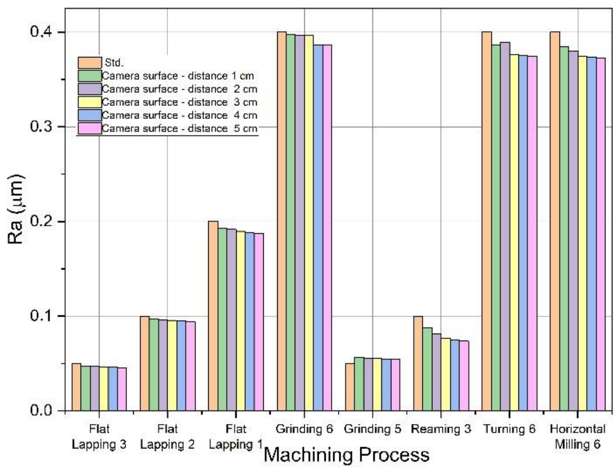

Fig. 5. Ra values obtained using the Nikon D3300 DSLR at camera–surface distances of 1–5 cm across eight ISO 2632 reference surfaces. Values are reported as mean ± standard deviation, where replicate measurements were available.

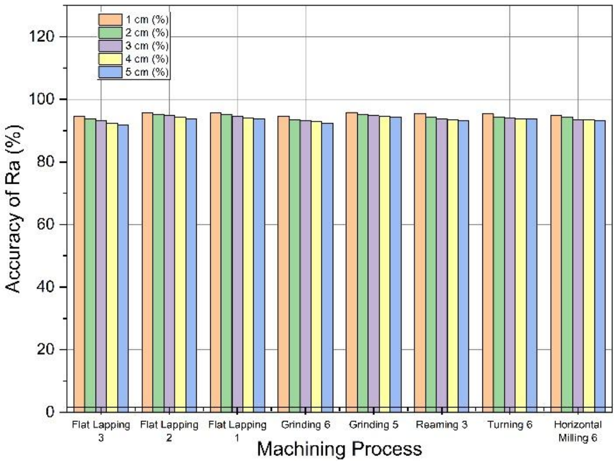

Fig. 6. Percentage accuracy of DSLR-based Ra measurements at camera–surface distances of 1–5 cm relative to the ISO 2632 certified reference values. Error bars represent the standard deviation from repeated measurements.

For the Flat Lapping 3 surface, the measured Ra value decreased from 0.0475 µm at 1 cm to 0.0471 µm at 2 cm, 0.0467 µm at 3 cm, 0.0461 µm at 4 cm, and 0.0456 µm at 5 cm. Across the eight reference surfaces, Ra accuracy decreased from 94.58–95.86% at 1 cm to 91.77–94.37% at 5 cm. This trend indicates that larger camera–surface distances tend to produce lower roughness estimates.

In this study, the calculated effective spatial resolution remained constant because the same calibrated region of interest (10 mm × 10 mm) was used across all DSLR distances. The corresponding spatial resolutions were 1.67 µm/pixel horizontally and 2.50 µm/pixel vertically, with a mean of 2.08 µm/pixel. Therefore, the observed decrease in accuracy should not be attributed to a change in the calculated µm/pixel value. Instead, it is more likely associated with distance-dependent optical effects, including reduced focus stability, lower image sharpness, weaker surface contrast, glare, and illumination variation. These effects may reduce the visibility of fine asperities and valleys, producing smoother reconstructed roughness profiles, especially on reflective metallic surfaces [23,25–28,32].

To summarize the distance-dependent DSLR results, Table 6 presents the calibrated ROI, mean effective spatial resolution, Ra accuracy range, and main interpretation for each camera–surface distance.

Table 6. Summary of DSLR distance effect on Ra accuracy and spatial resolution, showing calibrated ROI, mean effective spatial resolution, accuracy range, and main interpretation for each camera–surface distance.

Dist. [cm]	Calib. ROI [mm × mm]	Mean Res. [µm/pixel]	Ra Acc. Range [%]	Main Note
1	10 × 10	2.08	94.58–95.86	Highest accuracy
2	10 × 10	2.08	93.83–95.27	Slight decrease
3	10 × 10	2.08	93.24–94.78	Moderate decrease
4	10 × 10	2.08	92.46–94.51	Lower image stability
5	10 × 10	2.08	91.77–94.37	Lowest accuracy

As shown in Table 6, the calculated mean spatial resolution remained constant at 2.08 µm/pixel because the same calibrated ROI (10 mm × 10 mm) was used for all DSLR distances. However, Ra accuracy decreased progressively from 1 to 5 cm. Statistical analysis confirmed a significant effect of camera–surface distance on DSLR-based Ra estimation ($p < 0.05$). This result indicates that camera–surface distance influenced the DSLR roughness estimates, although the calculated spatial resolution remained constant. Therefore, the distance effect was mainly associated with optical image quality, including focus stability, image sharpness, illumination uniformity, surface contrast, and glare, rather than changes in the calculated spatial resolution [26–28].

This finding suggests that DSLR-based roughness estimation requires strict control of camera–surface distance, focus, illumination, and surface contrast, particularly when measuring fine roughness on reflective metallic surfaces [26– 28].

Figure 7 supports this interpretation by showing that fine surface texture became less distinct as the camera–surface distance increased. Although the calibrated spatial resolution remained constant within the selected ROI, usable image detail decreased due to optical degradation at greater distances. This explains the progressive underestimation of Ra and the reduction in measurement accuracy.

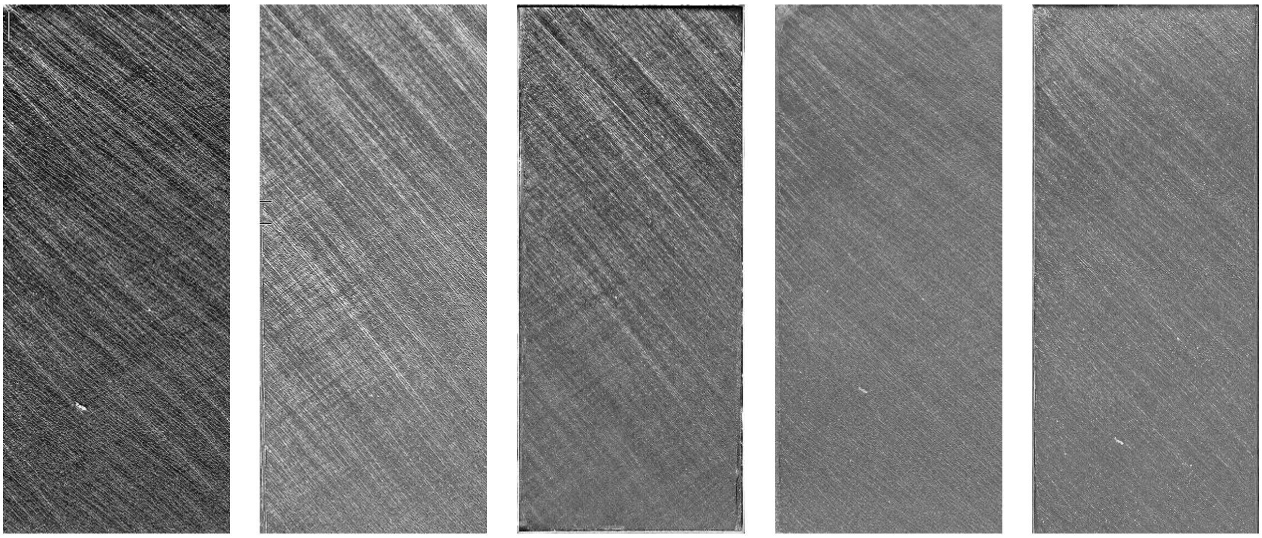

Fig. 7. Representative DSLR images acquired at camera–surface distances of (a) 1 cm, (b) 2 cm, (c) 3 cm, (d) 4 cm, and (e) 5 cm, showing reduced visibility of fine surface texture and contrast at larger distances.

To evaluate the statistical effect of camera–surface distance, the Ra values obtained at 1, 2, 3, 4, and 5 cm were compared across the eight ISO 2632 reference surfaces. If the data satisfied the normality assumption, repeated-measures ANOVA was applied. If normality was not satisfied, the Friedman test was used as a non-parametric alternative. Statistical significance was evaluated at $p < 0.05$. This analysis was used to determine whether the observed decrease in DSLR accuracy with increasing distance was statistically meaningful rather than only descriptive.

3.3 Comparison between Gwyddion and ImageJ software

The effect of image-processing software was evaluated by comparing roughness values obtained using Gwyddion and ImageJ. Figure 8 compares the Ra and Rz values obtained from both workflows, while Figure 9 presents the corresponding accuracy values. Overall, Gwyddion produced roughness values that were consistently closer to the certified ISO 2632 reference values than those obtained using ImageJ.

For the Flat Lapping 2 surface, which has certified values of Ra = 0.10 μm and Rz = 1.00 μm, Gwyddion yielded Ra = 0.0973 μm and Rz = 0.9647 μm. Under the same condition, ImageJ yielded Ra = 0.0954 μm and Rz = 0.9356 μm. Across the eight reference surfaces, Gwyddion achieved Ra accuracies of 95.76–97.86% and Rz accuracies of 94.44–97.04%, whereas ImageJ achieved Ra accuracies of 93.56–95.06% and Rz accuracies of 92.53–94.46%.

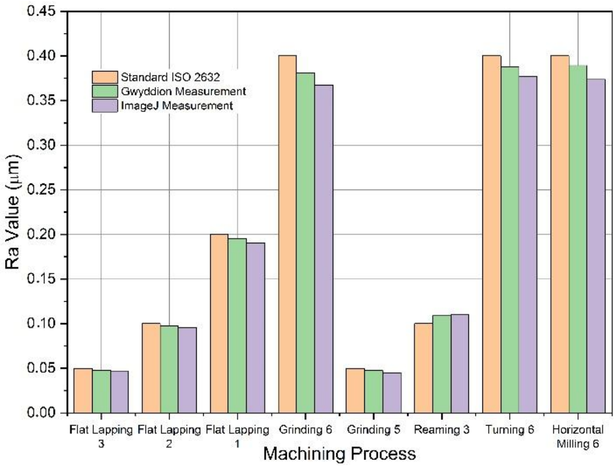

(a)

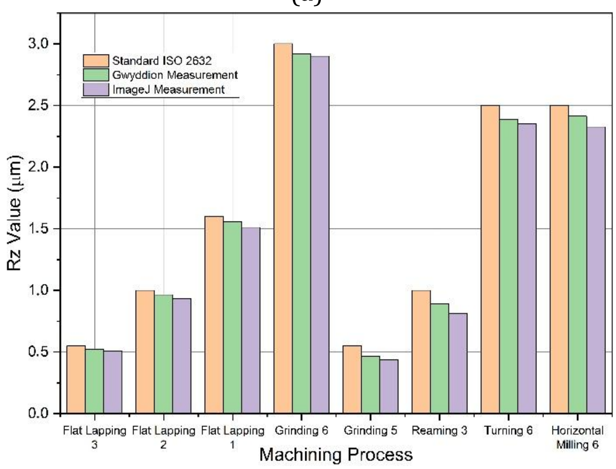

(b)

Fig. 8. Comparison of roughness values obtained using Gwyddion and ImageJ processing across eight ISO 2632 reference surfaces: (a) Ra and (b) Rz.

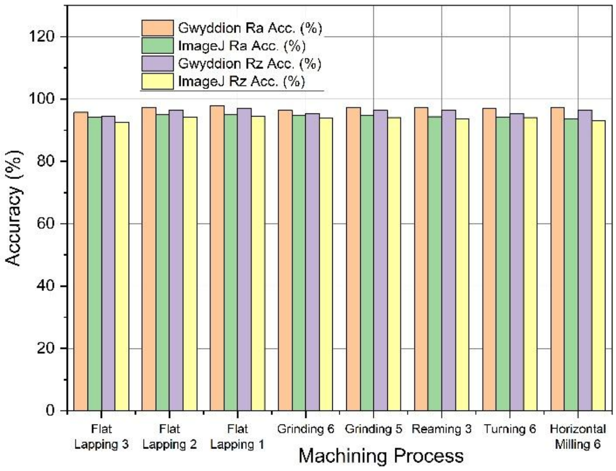

Fig. 9. Percentage accuracy of Gwyddion- and ImageJ-derived Ra and Rz values relative to ISO 2632 certified reference values. Error bars represent measurement variability where replicate measurements were available.

The closer agreement obtained using Gwyddion can be attributed to its profile-based processing workflow. Gwyddion supports spatial calibration, leveling, filtering, profile extraction, and roughness parameter calculation, making it more suitable for quantitative roughness evaluation. In contrast, ImageJ estimates roughness indirectly from grayscale intensity and threshold-based texture descriptors. Therefore, ImageJ-derived roughness values are more sensitive to illumination, contrast, threshold selection, focus stability, and metallic surface reflectivity [15, 17,21,22].

Statistical analysis confirmed that the difference between Gwyddion and ImageJ was significant for the software-based roughness comparison ($p < 0.05$). This result indicates that the image-processing workflow significantly affected the estimated Ra and Rz values. Therefore, Gwyddion was used as the primary workflow for quantitative roughness reporting, while ImageJ was interpreted as a lower-cost intensity-based screening approach. Similar image-processing-based roughness estimation approaches have been reported previously, but such methods require careful calibration because image-derived descriptors do not directly represent complete surface height information [19].

To summarize the software-based comparison, Table 7 presents the representative roughness values, accuracy ranges, and main interpretation for Gwyddion and ImageJ. The summary shows that Gwyddion provided a closer agreement with the ISO 2632-certified values, whereas ImageJ produced indirect intensity-based roughness estimates.

Table 7. Summary of software-based roughness measurement performance, showing representative roughness values, accuracy ranges, and main interpretation for Gwyddion and ImageJ workflows.

Software	Param.	Rep. Value [μm]	Acc. Range [%]	Main Note
Gwyddion	Ra	0.0973	95.76–97.86	Closest to standard
Gwyddion	Rz	0.9647	94.44–97.04	Profile-based extraction
ImageJ	Ra	0.0954	93.56–95.06	Intensity-based estimate
ImageJ	Rz	0.9356	92.53–94.46	More sensitive to the threshold

Note: Representative values were obtained from the Flat Lapping 2 surface. Gwyddion showed closer agreement with the ISO 2632-certified values, whereas ImageJ provided indirect intensity-based roughness estimates.

As shown in Table 7, Gwyddion produced higher accuracy than ImageJ for both Ra and Rz. This difference is attributed to Gwyddion's profile-based workflow, which includes calibration, leveling, filtering, and profile extraction. In contrast, ImageJ relies on grayscale intensity and threshold-based descriptors, making it more sensitive to illumination, contrast, threshold selection, focus stability, and metallic surface reflectivity [15,17,21,22].

3.4 Case study: Roughness measurement on mild steel plate

The validated optical workflow was applied to a mild steel plate from the Welding Laboratory to evaluate its ability to detect local variations in roughness on a shipbuilding-relevant steel surface. Roughness was evaluated along five independent measurement lines for both imaging systems. The resulting Ra values are presented in Table 8.

Table 8. Ra values measured along five independent lines on the mild steel plate using a microscope and DSLR images processed in Gwyddion.

No.	Measurement	Microscope [µm]	DSLR Camera [µm]
1	Line 1	0.4667	0.4428
2	Line 2	0.4826	0.4639
3	Line 3	0.4731	0.4322
4	Line 4	0.4817	0.4232
5	Line 5	0.4942	0.4524

The microscope-derived Ra values ranged from 0.4667 to 0.4942 µm, whereas the DSLR-derived Ra values ranged from 0.4232 to 0.4639 µm. For all five measurement lines, the microscope produced slightly higher Ra values than the DSLR, with differences of approximately 0.02–0.06 µm. This result indicates that the microscope was more sensitive to local surface variations, whereas the DSLR preserved the overall roughness trend but yielded slightly lower estimates of roughness.

As shown in Table 8, the microscope consistently produced slightly higher Ra values than the DSLR for all five measurement lines. This suggests that the microscope resolved local peak-and-valley features more effectively, whereas the DSLR produced smoother estimates of roughness. However, because no stylus profilometer measurement was performed on the same mild steel plate, these results should be interpreted as a laboratory-based optical comparison rather than proof of industrial equivalence.

Figure 10 shows representative roughness profiles obtained from microscope and DSLR images of the mild steel plate. The microscope-based profile shows higher local peak amplitudes and finer surface detail, while the DSLR-based profile follows the same general roughness trend with lower peak intensity. This difference is consistent with the microscope's higher optical resolution and more stable imaging configuration.

Figure 10 supports the quantitative results in Table 8. The microscope-based profile shows higher local peak amplitudes and finer surface detail, while the DSLR-based profile follows the same general trend with lower peak intensity. This confirms that both systems could detect local variations in roughness, but the microscope provided more detailed surface information.

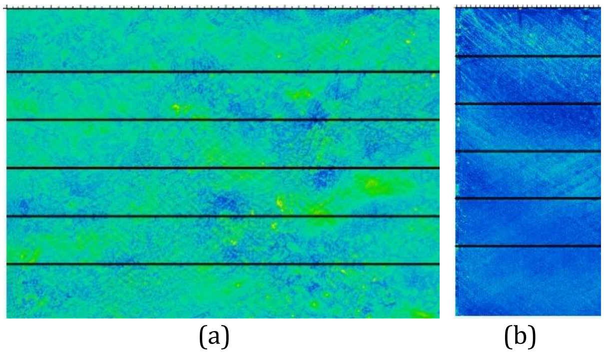

Fig. 10. Roughness profiles of the mild steel plate obtained from microscope and DSLR images: (a) comparison of measured profiles and (b) local profile features, showing higher peak amplitudes and finer detail in the microscope-based profile.

However, the mild steel measurement should be interpreted as a controlled laboratory case study rather than a full industrial validation. No direct stylus profilometer or other established roughness measurement technique was applied to the same mild steel specimen. Therefore, the present result should not be interpreted as evidence of equivalence between the optical workflow and standard industrial roughness instruments. The validation of the optical workflow in this study was based on the ISO 2632 reference plate, while the mild steel application was used to examine whether the calibrated optical workflow could detect local roughness variation on a shipbuilding-relevant substrate [30,31].

In addition, the ISO 2632 validation range was limited to fine reference surfaces with Ra values from 0.05 to 0.40 µm. Therefore, the present mild steel case study should not be generalized to blasted, corroded, coated, or fouled ship plates without further validation. Future work should compare the optical workflow directly with stylus profilometry or industrial optical profilometry on the same mild steel specimens, and extend the validation to more severe marine surface conditions.

These results show that both optical systems could detect variations in roughness on the mild steel specimen under controlled laboratory conditions. However, because no stylus profilometer or industrial optical profilometer was used on the same specimen, the results should be interpreted as a laboratory-based optical comparison rather than evidence of equivalence with standard industrial roughness measurement.

3.5 Summary of key quantitative findings

Across all experiments, the optical non-contact method achieved validation accuracy above 91% for both Ra and Rz under all tested configurations. The highest performance was obtained with microscope imaging and Gwyddion processing. Specifically, microscope-based measurements achieved Ra accuracy up to 97.20%, while Gwyddion achieved Ra accuracy up to 97.86% and Rz accuracy up to 97.04%. DSLR-based measurements also showed high accuracy, although performance decreased gradually as the camera–surface distance increased.

Overall, the results demonstrate that calibrated optical imaging can reproduce certified roughness values with high fidelity for finely machined metallic surfaces and can also detect small roughness differences on mild steel.

The figures and tables collectively support the validation and interpretation of the optical roughness workflow. Figure 1 and Table 1 define the ISO 2632 reference artifact and certified roughness values used for validation. Tables 2–4 describe the microscope and DSLR acquisition settings, including calibrated spatial resolution for the DSLR workflow. Figures 2–4 and Table 5 show that both microscope and DSLR imaging reproduced the certified roughness values with good agreement, although the microscope provided closer agreement and sharper peak-and-valley reconstruction.

Figures 5–7 and Table 6 demonstrate the effect of DSLR camera–surface distance. Although the calculated spatial resolution remained constant because the same calibrated ROI was used, Ra accuracy decreased with increasing distance, primarily due to distance-dependent optical effects, including focus stability, image sharpness, illumination uniformity, contrast, and glare. Figures 8–9 and Table 7 show that Gwyddion provided closer agreement with ISO 2632 reference values than ImageJ because it uses a profile-based workflow, whereas ImageJ provides indirect intensity-based estimates. Table 8 and Figure 10 show that both systems detected local roughness variation on the mild steel plate, but the microscope provided higher Ra values and finer profile details. Finally, Figure 11 summarizes the overall workflow and positions the method as a controlled-condition roughness assessment approach rather than a direct industrial replacement for standard roughness instruments.

4. DISCUSSION

4.1 Optical and processing factors affecting roughness estimation

This study demonstrates that calibrated optical imaging can estimate fine roughness on mild steel surfaces with high agreement against an ISO 2632 reference plate. The main finding is that measurement performance was governed not only by the nominal imaging device, but also by optical stability, camera–surface distance, illumination, surface reflectivity, and image-processing workflow. Therefore, the differences observed among the microscope, DSLR, Gwyddion, and ImageJ results should be interpreted as combined effects of optical acquisition and digital roughness extraction, rather than as simple differences in instrument accuracy.

The microscope produced the most consistent agreement with the certified reference values. This result can be explained by its more stable optical configuration, higher magnification, larger numerical aperture, and controlled illumination at the specimen plane. These factors improve the visibility of fine peak-and-valley features and reduce the risk of smoothing local asperities during image processing. In contrast, DSLR imaging is more sensitive to focus stability, image sharpness, exposure consistency, illumination uniformity, and surface reflectivity. For fine metallic surfaces, small changes in contrast or glare can reduce the visibility of micro-scale texture and lead to lower reconstructed roughness values [22–24].

The distance-dependent DSLR results further confirm the importance of optical acquisition control. In this study, the same calibrated region of interest was used for all camera–surface distances, so the calculated effective spatial resolution remained constant. Therefore, the decrease in DSLR accuracy with increasing distance should not be attributed to a change in the calculated μm/pixel value. Instead, it is more reasonably explained by distance-dependent optical degradation, including reduced focus stability, lower image sharpness, weaker texture contrast, non-uniform illumination, glare, and exposure variation. These effects can suppress fine asperity information and produce smoother profile estimates, particularly on reflective steel surfaces [25,26–28,32].

Illumination also played an important role in the reliability of image-based roughness estimation. Optical roughness workflows depend on the image's ability to preserve meaningful surface texture. If illumination is uneven, too weak, or affected by glare, grayscale and profile-like features may no longer consistently represent the actual surface condition. This issue is especially relevant for metallic ship plates because reflective surfaces can produce local brightness saturation and contrast loss. Therefore, DSLR-based roughness measurement should be considered reliable only under controlled acquisition conditions, including fixed distance, stable focus, consistent illumination, and calibrated image processing [26–28].

The comparison between Gwyddion and ImageJ shows that the image-processing workflow strongly affects the final roughness estimate. Gwyddion provided closer agreement with the certified values because it supports spatial calibration, leveling, filtering, profile extraction, and roughness parameter calculation. This profile-based workflow is more appropriate for quantitative roughness reporting. In contrast, ImageJ estimates roughness indirectly from grayscale intensity, thresholding, and texture descriptors. Consequently, ImageJ-derived values are more sensitive to illumination, contrast adjustment, threshold selection, focus quality, and surface reflectivity. ImageJ can therefore be useful as a low-cost screening tool, but it should not be interpreted as equivalent to profile-based roughness extraction without careful calibration [15,17,21,22].

4.2 Relevance to marine surface inspection

From a marine engineering perspective, the proposed workflow is relevant because surface roughness is associated with coating condition, fouling development, hydrodynamic resistance, and maintenance planning. Increased hull roughness can contribute to higher frictional resistance, ship resistance, and energy demand, while surface texture may also influence coating condition, coating degradation, and the development of biofouling [1–9,33]. However, the present study does not directly measure friction, wear, lubrication, coating adhesion, fouling growth, drag, or fuel consumption. Therefore, the results should be interpreted as roughness-based surface characterization that can support marine inspection decisions, not as direct evidence of tribological, coating, fouling, or hydrodynamic performance.

Figure 11 summarizes this interpretation by linking imaging configuration, image-processing workflow, roughness output, and controlled-condition marine surface inspection. The framework indicates that microscope imaging and Gwyddion processing are better suited to quantitative laboratory assessment, whereas DSLR imaging and ImageJ processing may support preliminary screening under controlled acquisition conditions. This distinction is important because shipyard environments involve variable lighting, surface contamination, surface curvature, coating condition, and operator-dependent camera positioning. These factors may reduce repeatability if the workflow is applied without strict calibration and acquisition control.

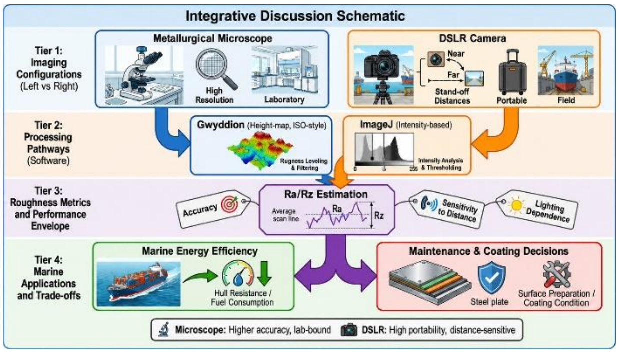

Fig. 11. Conceptual framework of the optical roughness workflow, linking imaging configuration, image-processing software, roughness estimation, and controlled-condition marine surface inspection.

Overall, the findings support the use of calibrated optical imaging for roughness-based surface characterization under controlled conditions. The microscope-Gwyddion workflow is more appropriate for quantitative laboratory assessment, whereas the DSLR-ImageJ workflow may support preliminary screening when imaging distance, focus, illumination, exposure, surface cleanliness, and calibration are carefully controlled. The proposed workflow should not be interpreted as a substitute for stylus profilometry, confocal microscopy, or industrial optical profilometry without further validation.

4.3 Practical implications for controlled roughness screening

The practical implication of this study is that calibrated optical imaging can support preliminary assessment of the roughness of fine or finished mild steel surfaces under controlled laboratory conditions. The microscope-based workflow is more suitable for quantitative roughness evaluation because it provides more stable imaging, higher optical resolution, and better preservation of local peak-and-valley information. In contrast, the DSLR-based workflow should be interpreted only as a potential screening-level approach when camera–surface distance, focus, illumination, exposure, surface cleanliness, and calibration are carefully controlled.

For practical inspection, DSLR imaging may help identify relative differences in surface roughness or support rapid preliminary assessment before more rigorous measurement is conducted. However, DSLR-derived roughness values should not be treated as direct substitutes for stylus profilometry, confocal microscopy, or industrial optical profilometry. The DSLR workflow relies on reference-calibrated optical texture information and remains sensitive to focus instability, glare, illumination non-uniformity, camera positioning, and metallic surface reflectivity [26–28]. Therefore, its use should be limited to controlled screening and comparative assessment rather than final acceptance testing or standard industrial reporting.

The findings may support marine maintenance planning by providing a non-contact method for monitoring fine surface condition, coating readiness, or local roughness variation on mild steel surfaces. Surface roughness is relevant to coating condition, fouling development, hydrodynamic resistance, ship resistance, energy consumption, and maintenance decisions [1–9,33]. However, the present results should not be interpreted as direct evidence of friction, wear, drag, fouling growth, coating adhesion, or fuel-consumption performance. These effects were not measured in this study.

The validation range also limits the practical applicability of the proposed workflow. The ISO 2632 reference plate used in this study covered fine surfaces with Ra values from 0.05 to 0.40 µm. Therefore, the findings should not be generalized to blasted, corroded, coated, or fouled ship surfaces without additional validation. These surface conditions are rougher, more heterogeneous, and more optically complex than the reference surfaces used in the present study. Further comparison with stylus profilometry or industrial optical profilometry on the same specimens is required before the method can be recommended for routine shipyard inspection [7,28,30,33].

4.4 Limitations and future work

Several limitations should be clearly acknowledged. First, the optical workflow was validated using an ISO 2632 roughness comparison plate. Still, no direct comparison with a stylus profilometer or industrial optical profilometer was performed on the same mild steel specimen. Therefore, the present results agree with the certified ISO 2632 reference surfaces but do not establish full equivalence with standard industrial roughness instruments on the actual shipbuilding steel substrate [28,30].

Second, the validation range was limited to fine reference surfaces with Ra values from 0.05 to 0.40 µm. This range represents fine or finished surfaces and does not represent rougher marine surfaces produced by blasting, corrosion, coating degradation, or biofouling. Therefore, the findings should not be generalized to blasted, corroded, coated, or fouled ship plates without additional validation on surfaces with broader and rougher Ra ranges [7,33].

Third, the mild steel case study was conducted on a single laboratory specimen under controlled imaging conditions. The results indicate that the calibrated optical workflow can detect local roughness variation on a mild steel surface. Still, they do not represent the variability of real shipyard or onboard inspection environments. Field conditions may include non-uniform illumination, surface contamination, glare, curved surfaces, coating residues, camera positioning variability, and unstable working distances. These factors can reduce the repeatability and accuracy of DSLR-based roughness estimation, particularly on reflective metallic surfaces [26–28].

Fourth, DSLR and ImageJ-based roughness values should be interpreted as reference-calibrated optical estimates rather than direct topographical measurements. Their reliability depends strongly on calibration quality, image sharpness, focus stability, illumination uniformity, exposure setting, threshold selection, and surface reflectivity. Therefore, DSLR imaging should be limited to controlled screening-level assessment and should not be used as a substitute for stylus profilometry, confocal microscopy, or industrial optical profilometry without further validation [26–28],30].

Future work should extend the validation to rougher and more heterogeneous marine steel surfaces, including blasted, corroded, coated, and fouled conditions [7,33]. Direct comparison with stylus profilometry and industrial optical profilometry should be performed on the same specimens to establish stronger metrological traceability and practical reliability [28,30]. In addition, future studies should evaluate the robustness of the optical workflow under shipyard-like lighting, surface contamination, camera-positioning variability, surface curvature, and larger inspection areas. These steps are necessary before the proposed method can be recommended for routine field inspection of ship plates.

5. CONCLUSION

This study evaluated the feasibility of non-contact optical roughness measurement on mild steel ship plates using a metallurgical microscope and a DSLR camera, with roughness extracted using Gwyddion and ImageJ. Validation against the ISO 2632 roughness comparison plate showed that the calibrated optical workflow could reproduce fine certified roughness values within the validation range of Ra = 0.05–0.40 µm. The microscope provided the most consistent agreement with the certified reference values. In contrast, Gwyddion yielded more accurate roughness estimates than ImageJ did, owing to its profile-based calibration, leveling, filtering, and roughness-extraction workflow.

The results indicate that calibrated optical imaging can support roughness-based surface characterization of fine or finished mild steel surfaces under controlled laboratory conditions. The microscope-based workflow is better suited for quantitative roughness evaluation due to its higher optical resolution and more stable imaging configuration. In contrast, DSLR imaging should be interpreted only as a potential screening-level approach when camera–surface distance, focus, illumination, exposure, surface cleanliness, and calibration are carefully controlled. DSLR-derived roughness values should not be considered a direct substitute for stylus profilometry, confocal microscopy, or industrial optical profilometry.

The practical relevance of the proposed workflow lies in its ability to support preliminary roughness assessment, coating-readiness evaluation, and maintenance-oriented surface inspection. However, this study did not directly measure friction, wear, lubrication, coating adhesion, fouling growth, drag, or fuel consumption. Therefore, the findings should be interpreted as roughness-based surface characterization rather than direct evidence of tribological or hydrodynamic performance.

This study has several limitations. The validation was limited to fine ISO 2632 reference surfaces, only one mild steel specimen was examined, and all measurements were performed under controlled laboratory conditions. No direct comparison with a stylus profilometer or industrial optical profilometer was performed on the same mild steel specimen. Therefore, the present findings should not be generalized to blasted, corroded, coated, or fouled ship surfaces without further validation. Future work should extend the validation to rougher and more heterogeneous marine steel surfaces. It should include direct comparison with stylus profilometry or industrial optical profilometry on the same specimens before the workflow can be recommended for routine shipyard inspection.

Acknowledgement

The authors gratefully acknowledge the support provided by the Department of Naval Architecture, Faculty of Engineering, Diponegoro University. The authors also thank the Laboratory for Engineering Design and Tribology, Faculty of Engineering, Department of Mechanical Engineering, Diponegoro University, for the facilities and technical support provided during this study.

REFERENCES

[1] P. Balcombe *et al.*, "How to Decarbonise International Shipping: Options for Fuels, Technologies and Policies," *Energy Conversion and Management*, vol. 182, pp. 72–88, 2019, doi: 10.1016/j.enconman.2018.12.080.

[2] G. Mallouppas and E. A. Yfantis, "Decarbonization in Shipping Industry: A Review of Research, Technology Development, and Innovation Proposals," *Journal of Marine Science and Engineering*, vol. 9, no. 4, p. 415, 2021, doi: 10.3390/jmse9040415.

[3] S. Song, S. Dai, Y. K. Demirel, M. Atlar, S. Day, and O. Turan, "Experimental and Theoretical Study of the Effect of Hull Roughness on Ship Resistance," *Journal of Ship Research*, vol. 65, no. 01, pp. 62–71, 2021, doi: 10.5957/josr.07190040.

[4] Z. Shepard, D. Meyer, K. Kurtz, A. Julien, V. Oyanedel-Craver, and L. Maranda, "Testing for Biofilm Release as a Function of Simulated Ship Speed Using a Calibrated Water Jet Device," *Journal of Coatings Technology and Research*, vol. 21, no. 5, pp. 1773–1781, 2024, doi: 10.1007/s11998-024-00934-3.

[5] P. Sinclair *et al.*, "A Computational Model for Microbial Colonization of an Antifouling Surface," *Frontiers in Microbiology*, vol. 13, 2022, doi: 10.3389/fmicb.2022.920014.

[6] I. K. Suastika *et al.*, "Characteristics of Drag Due to Streamwise Inhomogeneous Roughness," *Ocean Engineering*, vol. 223, p. 108632, 2021, doi: 10.1016/j.oceaneng.2021.108632.

[7] R. Akbar, I. K. Suastika, and I. K. Aria Pria Utama, "Effects of Homogeneous and Inhomogeneous Roughness on the Ship Resistance," *CFD Letters*, vol. 17, no. 3, pp. 77–94, 2025, doi: 10.37934/cfdl.17.3.7794.

[8] W. Choi *et al.*, "Resistance and speed penalty of a naval ship with hull roughness," *Ocean Engineering*, vol. 312, p. 119058, Nov. 2024, doi: 10.1016/j.oceaneng.2024.119058.

[9] X. Zeng, X. Guo, and A. Yin, "Research on the Impact of Local Hull Roughness on Resistance and Energy Consumption Based on CFD and Ship Operation Data," *J. Mar. Sci. Eng.*, vol. 13, no. 9, 2025, doi: 10.3390/jmse13091675.

[10] N. Geier and C. Pereszlai, "Analysis of Characteristics of Surface Roughness of Machined CFRP Composites," *Periodica Polytechnica Mechanical Engineering*, vol. 64, no. 1, pp. 67–80, 2020, doi: 10.3311/ppme.14436.

[11] K. Grochalski, M. Wieczorowski, P. Pawlus, and J. H'roura, "Thermal Sources of Errors in Surface Texture Imaging," *Materials*, vol. 13, no. 10, p. 2337, 2020, doi: 10.3390/ma13102337.

[12] K. Grochalski, D. Podbereska, M. Wieczorowski, R. Talar, and W. Graboń, "Selected Errors in Spatial Measurements of Surface Asperities," *Materials*, vol. 17, no. 12, p. 2918, 2024, doi: 10.3390/ma17122918.

[13] I. S. Rout, P. P. Pandian, A. Raj, A. M. Rego, and S. P. Panigrahi, "Investigation on a Real Time Monitoring System with a Non-contact Device to Minimize Surface Roughness on Metal pieces," *Journal of Mines Metals and Fuels,* pp. 109–116, Jan. 2026, doi: 10.18311/jmmf/2026/50342.

[14] P. O. Cubillos, V. O. d. Santos, A. L. A. Pizzolatti, A. D. O. Moré, and Carlos Rodrigo de Mello Roesler, "Surface Finish of Total Hip Arthroplasty Implants: Are We Evaluating and Manufacturing Them Appropriately?," *Journal of Testing and Evaluation*, vol. 49, no. 6, pp. 4550–4559, 2021, doi: 10.1520/jte20200357.

[15] J. Caja, A. S. Lobera, P. Maresca, T. F. Pareja, and C. Wang, "Some Considerations About the Use of Contact and Confocal Microscopy Methods in Surface Texture Measurement," *Materials*, vol. 11, no. 8, p. 1484, 2018, doi: 10.3390/ma11081484.

[16] A. Khavieya, G. V. BhanuTeja, S. Chowdhury, N. Arunachalam, and A. R. Ganesan, "Quantification of Surface Roughness Using Fringe Projection Profilometry for Metallic Machined Surfaces," *Journal of Tribology*, vol. 147, no. 11, p. 114202, Nov. 2025, doi: 10.1115/1.4068171.

[17] N. Lishchenko, G. E. O'Donnell, and M. Culleton, "Contactless Method for Measurement of Surface Roughness Based on a Chromatic Confocal Sensor," *Machines*, vol. 11, no. 8, p. 836, 2023, doi: 10.3390/machines11080836.

[18] D. Patel and M. B. Kiran, "Non-Contact Surface Roughness Measurement Using Laser Speckle Technique," in *Iop Conference Series Materials Science and Engineering*, vol. 895, no. 1, p. 012007, Jul. 2020, doi: 10.1088/1757-899x/895/1/012007.

[19] J. S. Vishwanatha *et al.*, "Image-processing-based model for surface roughness evaluation in titanium based alloys using dual tree complex wavelet transform and radial basis function neural networks," *Sci Rep*, vol. 14, no. 1, p. 28261, Nov. 2024, doi: 10.1038/s41598-024-75194-7.

[20] E. S. Hadi *et al.*, "Study on the Effect of Laser Cleaning Power and Scanning Frequency on Surface Properties and Coating Adhesion of ASTM A36 Steel," *Tribology in Industry*, vol. 47, no. 4, pp. 732–742, Dec. 2025, doi: 10.24874/ti.1754.09.24.10.

[21] K. Paľová, T. Kelemenová, and M. Kelemen, "Measuring Procedures for Evaluating the Surface Roughness of Machined Parts," *Applied Sciences*, vol. 13, no. 16, p. 9385, 2023, doi: 10.3390/app13169385.

[22] C. A. Mack, J. Severi, M. Zidan, D. D. Simone, and G. F. Lorusso, "Unbiased Roughness Measurements From Low Signal-to-Noise Ratio Scanning Electron Microscope Images," *Journal of Micro/Nanopatterning Materials and Metrology*, vol. 22, no. 02, Dec. 2022, doi: 10.1117/1.jmm.22.2.021006.

[23] J. R. Abbott and H. Zhu, "3D Optical Surface Profiler for Quantifying Leaf Surface Roughness," *Surface Topography Metrology and Properties*, vol. 7, no. 4, p. 045016, 2019, doi: 10.1088/2051-672x/ab4cc6.

[24] Y. Chen, H. Li, Z. Zhu, and C. Zhao, "A Method for Achieving Nanoscale Visual Positioning Measurement Based on Ultra-Precision Machining Microstructures," *Micromachines*, vol. 14, no. 7, p. 1444, 2023, doi: 10.3390/mi14071444.

[25] H. Altamar-Mercado, A. Patiño-Vanegas, and A. G. Marrugo, "Robust 3D Surface Recovery by Applying a Focus Criterion in White Light Scanning Interference Microscopy," *Applied Optics*, vol. 58, no. 5, 2019, doi: 10.1364/ao.58.00a101.

[26] J. Ružbarský, "The Influence of the Wavelength of Laser Light on the Non-Contact Measurement of the Roughness of Shiny Cut Surfaces on Stainless Steel A304 Material," *Applied Sciences*, vol. 14, no. 6, p. 2420, 2024, doi: 10.3390/app14062420.

[27] J. Ružbarský, "The Difficulty of Measuring the Roughness of Glossy Surfaces Using the Triangulation Principle," *Applied Sciences*, vol. 13, no. 8, p. 5155, 2023, doi: 10.3390/app13085155.

[28] X. Xu, S. Hagemeier, and P. Lehmann, "Outlier Elimination in Rough Surface Profilometry With Focus Variation Microscopy," *Metrology*, vol. 2, no. 2, pp. 263–273, 2022, doi: 10.3390/metrology2020016.

[29] G. Mitaľ, J. Dobránsky, J. Ružbarský, and Š. Olejárová, "Application of Laser Profilometry to Evaluation of the Surface of the Workpiece Machined by Abrasive Waterjet Technology," *Applied Sciences*, vol. 9, no. 10, p. 2134, 2019, doi: 10.3390/app9102134.

[30] A. Mínguez-Martínez, P. Maresca, J. Caja, and J. d. Vicente, "Results of a Surface Roughness Comparison Between Stylus Instruments and Confocal Microscopes," *Materials*, vol. 15, no. 16, p. 5495, 2022, doi: 10.3390/ma15165495.

[31] A. Pappas, L. Newton, A. Thompson, and R. Leach, "Review of material measures for surface topography instrument calibration and performance verification," *Meas. Sci. Technol.*, vol. 35, no. 1, p. 012001, Jan. 2024, doi: 10.1088/1361-6501/acf1b9.

[32] M. S. Nielsen, I. Nikolov, E. K. Kruse, J. Garnæs, and C. Madsen, "Quantifying the Influence of Surface Texture and Shape on Structure From Motion 3D Reconstructions," *Sensors*, vol. 23, no. 1, p. 178, 2023, doi: 10.3390/s23010178.

[33] T. Veeranah and Y. Seechurn, "Investigating Coating Adherence on S275JR Carbon Steel Under Cyclic Corrosion," *Surface Engineering*, vol. 41, no. 6, pp. 695–710, 2025, doi: 10.1177/02670844251356710.